Top quark effective couplings from top-pair tagged photoproduction in pe^- collisions

Antonio O. Bouzas and F. Larios
Departamento de Física Aplicada, CINVESTAV-IPN
Carretera Antigua a Progreso Km. 6, Apdo. Postal 73 "Cordemex"
Mérida 97310, Yucatán, México

Received 15 March 2023; accepted 16 April 2023

We summarize the quantitative results of our analysis [1] of top-pair photoproduction in semileptonic mode in pe collisions at the LHeC and FCC-he. We define three photoproduction regions, based on the rapidity acceptance range of the electron tagger, that provide different degrees of sensitivity to top-quark effective couplings. We focus on the $t\bar{t}\gamma$ dipole couplings and the left-handed vector tbW coupling, for which we determine limits at both energies in the different photoproduction regions. We find that the LHeC and FCC-he will yield tight direct bounds on top dipole moments, greatly improving on current direct limits from hadron colliders, and direct limits on the tbW coupling as restrictive as those expected from the HL-LHC. We also consider indirect limits from $b \to s\gamma$ branching ratio and CP asymmetry, that are well known to be very sensitive probes of top electromagnetic dipole moments.

Keywords: ***top-quark photoproduction electron-proton-collider***

arXiv:2303.10286v1 [hep-ph] 17 Mar 2023

1 Introduction

Future pe^- colliders, such as the Large Hadron-electron Collider (LHeC) and the Future Circular Collider (FCC-he), will have among their most important areas of research the study of the top quark effective couplings to the Higgs and the electroweak bosons [2]. Indeed, the top quark effective couplings constitute a phenomenological research area of great interest [3,4]. Top-pair and single-top production at the LHeC are very good probes for charged-current (CC) tbW and neutral-current (NC) ttZ effective couplings [5, 6]. Also, anomalous magnetic and electric dipole moments of the top quark can be very well probed through top-pair photoproduction in electron-proton collisions [7–9].

In our recent paper [1] we obtain limits on the top-quark anomalous electromagnetic dipole moments and its left-handed vector tbW coupling, in the context of the Standard Model Effective Field Theory (SMEFT), by means of Monte Carlo simulations including parton showering and hadronization, and fast detector simulation, for both the LHeC and the FCC-he. We compute the photoproduction cross section in tree-level QED, taking the complete kinematics into account, including the scattered-electron transverse momentum. This allows us to determine the phase-space region where the photoproduction process is sensitive to the top anomalous dipole moments, and that in which it is sensitive to the anomalous tbW coupling.

Also studied in [1] are the indirect limits on top dipole moments from the decays $B \to X_s\gamma$. We update our previous results [10] for those limits, and discuss in detail the fact that there are currently two different sets of such limits, based on two incompatible theoretical computations [11, 12] of the new physics contributions to the branching ratio for $B \to X_s\gamma$ and its associated CP asymmetry.

In this note we discuss the quantitative results from [1] on direct limits on the anomalous top dipole moments and left-handed vector tbW coupling, and comment also on the indirect limits obtained there. We discuss experimental limits by the CMS collaboration on tbW couplings [13], as well as the very recent limits on top dipole moments [14] which were not included in [1]. We consider also the ATLAS collaboration projections on limits on top dipole moments for the HL-LHC [15].

A number of important issues discussed in [1] are not covered here for reasons of space. We point out among them, an extensive (and hopefully exhaustive) analysis of background processes, a summary of all global SMEFT top-quark analyses to date, and an in-depth discussion of the computation of indirect limits on anomalous couplings based on $B \to X_s\gamma$. We refer the reader to [1] for a comprehensive treatment of those topics.

This note is organized as follows. In section 2 we discuss the dimension-six SMEFT basis operators relevant to this work. In section 3 we discuss the top-pair photoproduction process in pe^- collisions in the SM, and its Monte Carlo simulation and computation. In section 4 we present our limits on top anomalous effective couplings, and compare them to those obtained and projected by experimental collaborations. Finally, in section 5, we give our final remarks.

2 Effective SM Lagrangian

The effective Lagrangian for the SM extended by dimension-six gauge-invariant operators is of the form,

$$\mathcal{L} = \mathcal{L}_{\rm SM} + \frac{1}{\Lambda^2}\sum_{\mathcal{O}}(\widehat{C}_{\mathcal{O}}\mathcal{O} + \text{h.c.}) + \cdots , \qquad (1)$$

where $\mathcal{O}$ denotes the dimension-six effective operators, Λ is the new-physics scale, and the ellipsis refers to higher-dimensional operators. It is understood in (1) that the addition of the Hermitian conjugate, denoted $+\text{h.c.}$ in the equa-

tion, is applicable only to non-Hermitian operators. Throughout this paper we use the dimension-six effective operators from the Warsaw operator basis [16]. In particular, we use the same sign convention for covariant derivatives as in [7, 16], namely, $D_\mu = \partial_\mu + ieA_\mu$ for the electromagnetic coupling. However, we adopt the operator normalization defined in [17] (see also [18]), where a factor y_t is attached to an operator for each Higgs field it contains, and a factor g (g') for each $W_{\mu\nu}$ ($B_{\mu\nu}$) field-strength tensor. The Wilson coefficients in (1) are denoted $\widehat{C}$, since we will denote C the coefficients associated with the original operator basis [16]. In fact, it will be convenient in what follows to express our results in terms of the modified dimensionless couplings

$$\widetilde{C}_{\mathcal{O}} = \widehat{C}_{\mathcal{O}} \frac{v^2}{\Lambda^2}, \tag{2}$$

where v is the Higgs-field vacuum expectation value. At tree level the coupling constants $\widetilde{C}_{\mathcal{O}}$ are independent of the scale Λ. We denote complex couplings as $\widetilde{C}_{\mathcal{O}} = \widetilde{C}_{\mathcal{O}\,r} + i\widetilde{C}_{\mathcal{O}\,i}$.

There are seven operators in the basis [16] that couple electroweak bosons and third family quarks. One of them, $Q^{33}_{\varphi u}$, does not contribute to the photoproduction process. Other three of them, $Q^{33}_{\varphi ud}$, Q^{33}_{uW}, Q^{33}_{dW}, are strongly limited by W-helicity fractions in $t\bar{t}$ production and decay at the LHC and HL-LHC, while the expected sensitivity of the top-pair photoproduction process to them is expected to be low. For these reasons, we do not consider them further. Of the three operators remaining, one linear combination, $Q^{(+)33}_{\varphi q} = Q^{(3)33}_{\varphi q} + Q^{(1)33}_{\varphi q}$, is strongly constrained by b-physics at LEP and SLAC electron–positron colliders. Therefore, we focus our analysis on the two operators $\mathcal{O}^{33}_{uB}$ and $\mathcal{O}^{(-)33}_{\varphi q}$. Expanding these operators in physical fields yields, with the conventions discussed above:

$$\begin{aligned}
\mathcal{O}^{33}_{uB} &= y_t g' Q^{33}_{uB} = \sqrt{2} y_t e (v+h)(\partial_\mu A_\nu - \tan\theta_W \partial_\mu Z_\nu)\, \bar{t}_L \sigma^{\mu\nu} t_R \,, \\
\mathcal{O}^{(-)33}_{\varphi q} &= \mathcal{O}^{(3)33}_{\varphi q} - \mathcal{O}^{(1)33}_{\varphi q} = -y_t^2 Q^{(-)33}_{\varphi q} \\
&= -y_t^2 \frac{g}{\sqrt{2}} (v+h)^2 \left(W^+_\mu \bar{t}_L \gamma^\mu b_L + W^-_\mu \bar{b}_L \gamma^\mu t_L \right) - y_t^2 \frac{g}{c_W} (v+h)^2 Z_\mu \bar{t}_L \gamma^\mu t_L \,,
\end{aligned} \tag{3}$$

where Q^{33}_{uB}, $Q^{(-)33}_{\varphi q}$ are the basis operators defined in [16]. Notice that both operators $\mathcal{O}^{33}_{uB}$ and $\mathcal{O}^{(-)33}_{\varphi q}$ are $O(g^1)$ with respect to the weak coupling constant, which makes the definitions (3) consistent from the point of view of perturbation theory. We stress here the definition $\mathcal{O}^{(-)33}_{\varphi q} = \mathcal{O}^{(3)33}_{\varphi q} - \mathcal{O}^{(1)33}_{\varphi q}$ we use, since sometimes in the literature the opposite sign is used. The effective Lagrangian used throughout this paper results from substituting (3) and (2) in the Lagrangian (1). It is convenient to record here the relation between the Wilson coefficients in the form (2) and those associated with the original basis [16] (see also [19]),

$$\begin{aligned}
C^{33}_{uB} &= \frac{\Lambda^2}{v^2} y_t g' \widetilde{C}^{33}_{uB} = 5.906 \widetilde{C}^{33}_{uB} \,, \\
C^{(-)33}_{\varphi q} &= -\frac{\Lambda^2}{v^2} y_t^2 \widetilde{C}^{(-)33}_{\varphi q} = -16.495 \widetilde{C}^{(-)33}_{\varphi q} \,.
\end{aligned} \tag{4}$$

The numerical values in this equation arise from the parameters $\Lambda = 1$ TeV, $v = 246$ GeV, $g' = 0.358$, $g = 0.648$, $y_t = 1$.

It is common practice in the literature to write the anomalous interactions in terms of form factors. We adopt here the definition of top electromagnetic dipole moments given in eq. (2) of [7], and the CC vertex form factors from eq. (7.1) of [13]. Comparing those equations (which are summarized in eq. (5) of [1]), with (1), (2), (3), yields the tree-level relations,

$$\kappa = 2 y_t^2 \widetilde{C}^{33}_{uB\,r}, \qquad \widetilde{\kappa} = 2 y_t^2 \widetilde{C}^{33}_{uB\,i}, \qquad \delta f_V^L = y_t^2 \widetilde{C}^{(-)33}_{\varphi q} \,. \tag{5}$$

These particularly simple relations are a consequence of eq. (2) and the operator normalization discussed in the text immediately above that equation. We see from (5), in particular, that for all practical purposes $\delta f_V^L = \widetilde{C}^{(-)33}_{\varphi q}$.

3 Top-pair photoproduction in the SM

We are interested in top-pair photoproduction in pe^- collisions in the semileptonic decay channel which, at parton level, leads to the seven-fermion final states,

$$g\, e^- \to e^- t\bar{t} \to e^- b\ell^+\nu_\ell \bar{b}\bar{q}_u q_d + e^- b q_u \bar{q}_d \bar{b}\ell^-\bar{\nu}_\ell, \tag{6}$$

with $q_u = u, c$, $q_d = d, s$, $\ell = e, \mu$. The set of Feynman diagrams for this process in the photoproduction region in unitary gauge in the SM with Cabibbo mixing is shown in figure 1. We consider the top-pair photoproduction process defined by the diagrams in that figure our signal process.

We can divide the set of diagrams in figure 1 into two subsets: the first subset includes diagrams (a), (b), containing three internal top lines, and the second one comprises the remaining diagrams, (c)–(i), containing two internal top lines. The second subset is necessary to preserve electromagnetic gauge invariance in the phase-space regions where t or

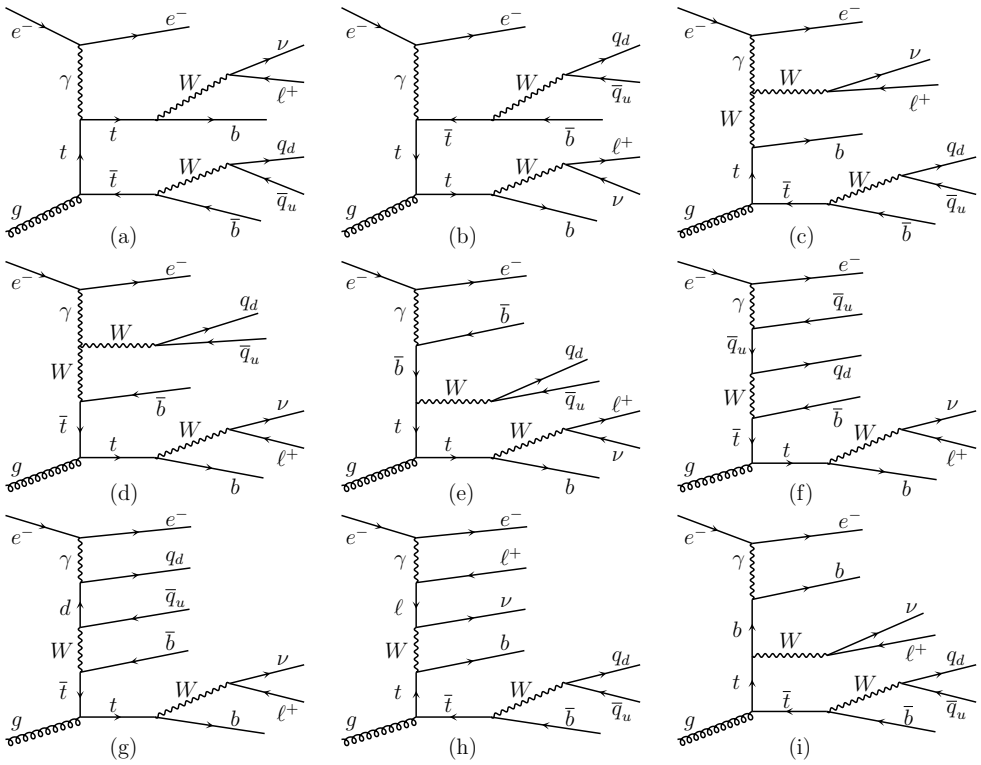


FIGURE 1. Unitary-gauge Feynman diagrams for the photoproduction of a top pair in semileptonic mode, see eq. (6). All diagrams for the final state $e^- b\ell^+\nu_\ell \bar{b}\bar{q}_u q_d$ are shown. Diagrams (c)–(i) are necessary to preserve electromagnetic gauge invariance when t, W are off shell.

W lines are off shell. There is, in fact, strong destructive interference between the two subsets in the photoproduction region, such that the total cross section computed with all the diagrams is smaller than the cross sections obtained from (a), (b) or (c)–(i) separately, by a factor 10–25 depending on the cuts used in the computation.

We must consider also other processes with the same final state as (6), which constitute irreducible backgrounds. Particularly important is the associate tbW photoproduction, in which bW does not originate in a top decay. The Feynman diagrams for tbW production are given in figure 2 of [1]. This process turns out to be the dominant background to the signal process (6). Several other irreducible and reducible backgrounds are discussed in sections 3 and 5 of [1].

We compute the tree-level cross section for top-pair photoproduction and its backgrounds with MadGraph5_aMC@NLO version 2.6.3 [20], together with Pythia version 6.428 [21] and Delphes version 3.4.2 [22]. The parameters of the simulation are described in section 4 of [1], as are the details of the top-reconstruction method, and the event-selection cuts. We are led to define three photoproduction regions, characterized by the rapidity of the scattered electron,

$$\begin{aligned} PhP_I: &\quad -4.741 < y(e^-) < -3.0, \\ PhP_{II}: &\quad -5.435 < y(e^-) < -3.0, \\ PhP_{III}: &\quad -6.215 < y(e^-) < -3.0. \end{aligned} \tag{7}$$

As discussed in detail in [1], the sensitivity to $\widetilde{C}_{uB}^{33}$ is highest in PhP_I and lowest in PhP_{III}, and the sensitivity to $\widetilde{C}_{\varphi q}^{(-)33}$ is highest in PhP_{III} and lowest in PhP_I. Both sensitivities are intermediate in PhP_{II}.

With the phase-space cuts specified in section 4 of [1], the cross sections for the $t\bar{t}$ photoproduction signal process (6), figure 1, and the tbW irreducible background, are found to be as follows,

	LHeC			FCC-he		
[fb]	PhP_I	PhP_{II}	PhP_{III}	PhP_I	PhP_{II}	PhP_{III}
$t\bar{t}$	0.40	0.73	1.32	4.28	6.19	10.51
tbW	0.041	0.083	0.16	0.44	0.71	1.42

, (8)

expressed in femtobarns. We notice here that the tbW background has cross section at the parton level that is roughly 20% of the signal cross section at the LHeC, and roughly 35% at the FCC-he, the precise number depending on the photoproduction region. We designed the phase-space cuts to reduce this background to levels below 15%. As seen in (8), the tbW background is 10% of the signal in region PhP_I

and 11.3% in PhP_{II} at both the LHeC and FCC-he. In region PhP_{III} we have 12.2% at the LHeC and 13.5% at the FCC-he. This tbW background proves to be the most difficult one to control.

4 Results for effective couplings

In this section we summarize the main results for the effective-coupling limits from [1].

4.1 Bounds on $\widetilde{C}_{\varphi q}^{(-)33}$

The largest sensitivity to $\widetilde{C}_{\varphi q}^{(-)33}$ is obtained in region PhP_{III}. Indeed, the anomalous coupling $\widetilde{C}_{\varphi q}^{(-)33}$ constitutes a perturbation δf_V^L to the SM charged-current coupling $f_V^L = 1 + \delta f_V^L$ and, therefore, it also perturbs the cancellation among diagrams discussed above in section 3. Thus, the sensitivity is largest in region PhP_{III} where the cancellation is strongest. We obtain limits for $\widetilde{C}_{\varphi q}^{(-)33}$ at the LHeC and FCC-he energies, in photoproduction region III, at one- and two-sigma levels, assuming a measurement uncertainty of 12%,

$$\begin{aligned} 68\%\,\text{C.L.}: &\quad -0.039 < \delta f_V^L < 0.035\,, \\ 95\%\,\text{C.L.}: &\quad -0.083 < \delta f_V^L < 0.067\,. \end{aligned} \tag{9}$$

These limits are obtained from a single total cross section value, with no other observable involved. We express them in terms of δf_V^L to compare them to the limits reported by CMS; from fig. 6 of [13] we get,

$$\begin{aligned} 68\%\,\text{C.L.}: &\quad -0.024 < \delta f_V^L < 0.094\,, \\ 95\%\,\text{C.L.}: &\quad -0.062 < \delta f_V^L < 0.132\,. \end{aligned} \tag{10}$$

By taking interval length as a measure of sensitivity, we see that both limits in (9) are significantly stronger than those in (10).

4.2 Bounds on $\widetilde{C}_{uB}^{33}$: single-coupling bounds

The largest sensitivity to $\widetilde{C}_{uB}^{33}$ is obtained in region PhP_I. This is due to the fact that the SM is close to an infrared divergence at $Q^2 = 0$ and, therefore, as Q^2 decreases the SM cross section grows much faster than the dipolar cross section, which is infrared finite. This causes the sensitivity to both $\widetilde{C}_{uB\,r}^{33}$, $\widetilde{C}_{uB\,i}^{33}$ to decrease as we go from PhP_I to PhP_{III}. We obtain limits on $\widetilde{C}_{uB}^{33}$ at the LHeC and FCC-he energies, in photoproduction region I, at one- and two-sigma levels, assuming a measurement uncertainty of 12%,

$$\begin{aligned} 68\%\,\text{C.L.}: &\quad \begin{cases} -0.24 < C_{uB\,r}^{33} < 0.29\,, \\ -0.89 < C_{uB\,i}^{33} < 0.89\,, \end{cases} \\ 95\%\,\text{C.L.}: &\quad \begin{cases} -0.45 < C_{uB\,r}^{33} < 0.65\,, \\ -1.24 < C_{uB\,i}^{33} < 1.24\,. \end{cases} \end{aligned} \tag{11}$$

The limits on $\widetilde{C}_{uB\,r}^{33}$, which is proportional to the magnetic dipole moment, are asymmetric because of the interference with the SM. Also for that reason, they are stronger than those on the imaginary part. Since the electric dipole moment operator is CP odd, the interference with the SM is very small, and the limits on $\widetilde{C}_{uB\,i}^{33}$ are symmetric.

We compare the limits (11) with those projected for the HL-LHC by the ATLAS collaboration [15], from the radiative top-pair production and decay process $pp \to t\bar{t}\gamma$,

$$95\%\,\text{C.L.}: \qquad -0.5 < C_{uB\,r}^{33} < 0.3\,. \tag{12}$$

These are somewhat stricter than those we obtain, (11), based on interval length. We remark, however, that the ATLAS projections are based on two channels ($\ell\ell$ and ℓj), and involve the total cross section and two differential cross sections each one spanning about six bins. There are, in total, about a dozen measurements involved in the limits (12), whereas (11) are based on a single observable, the total cross section.

The limits set on C_{uB}^{33} by the ATLAS and CMS collaborations from measurements of $t\bar{t}\gamma$ production are nowadays incorporated into global analyses; we refer to [1] for a detailed review of those. Very recently, the CMS collaboration [14] has measured the total cross section for $pp \to t\bar{t}\gamma$, as well as two differential cross sections ($d\sigma/dp_{T\gamma}$, $d\sigma/d\eta_\gamma$), in two reaction channels ($\ell\ell$ and ℓj). The limits obtained from the dilepton channel,

$$95\%\,\text{C.L.}: \qquad \begin{cases} -1.08 < C_{uB\,r}^{33} < 1.10\,, \\ -1.08 < C_{uB\,i}^{33} < 1.21\,, \end{cases} \tag{13}$$

are significantly weaker than ours, (11), by interval length. The limits obtained from a combination of both channels are reported to be,

$$95\%\,\text{C.L.}: \qquad \begin{cases} -0.64 < C_{uB\,r}^{33} < 0.75\,, \\ -0.75 < C_{uB\,i}^{33} < 0.79\,, \end{cases} \tag{14}$$

and are substantially stronger than for each separate channel. The limits (14) are only slightly weaker than (11) for $\widetilde{C}_{uB\,r}^{33}$, but definitely stronger for $\widetilde{C}_{uB\,i}^{33}$. As is the case for the limits (12), the strong limits (14) are the result of combining more than a dozen observables: the total cross section and two differential cross sections, for two reaction channels.

4.3 Bounds on $\widetilde{C}_{uB}^{33}$: allowed two-coupling regions

In figure 2 we show the allowed regions in the κ–$\tilde{\kappa}$ plane, determined by the top-pair photoproduction cross section at both the LHeC and FCC-he energies, in region PhP_I at 68% C.L. These can be related to $\widetilde{C}_{uB}^{33}$ through (5), and to C_{uB}^{33} through (4). The allowed regions, given by the circular coronas, correspond to the assumed measurement uncertainties $\varepsilon_{\text{exp}} = 12$, 15, 18% in different colors as indicated in the figure caption. Also seen in figure 2 is that the annular allowed regions obtained at the FCC-he are somewhat smaller than those at the LHeC energy. We notice, however, that both sets

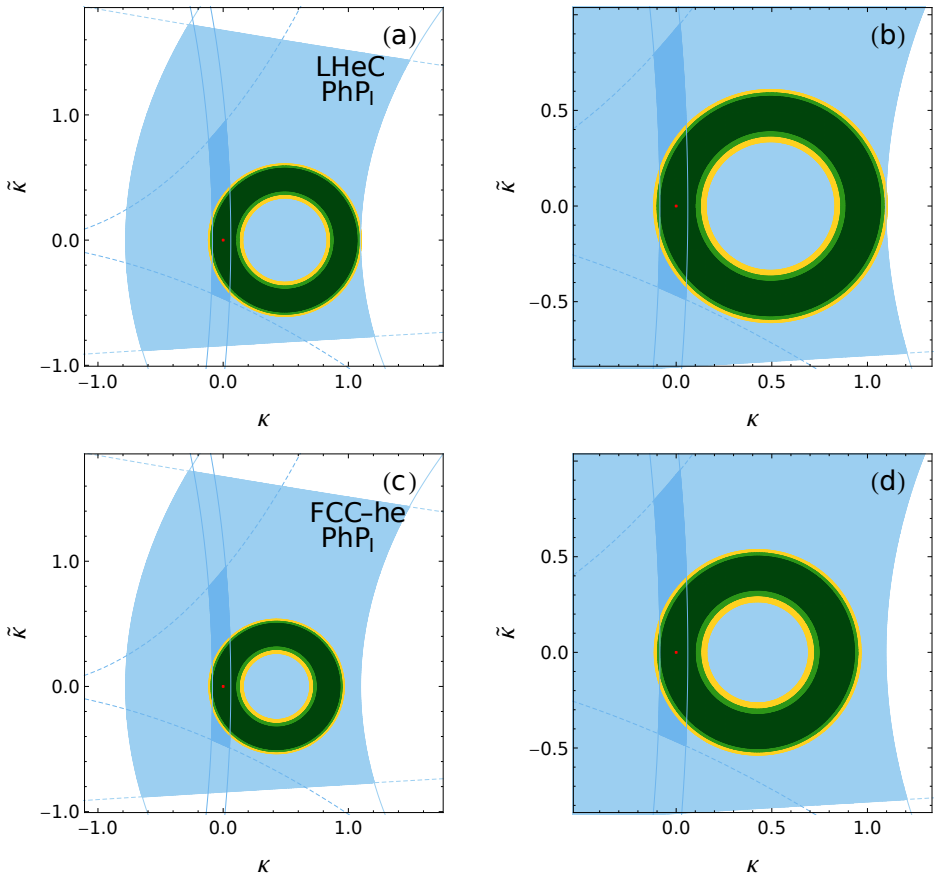


FIGURE 2. Allowed regions for the top quark dipole moments κ and $\widetilde{\kappa}$ at (a),(b) the LHeC and (c),(d) the FCC-he. Panels (a), (c) display a global view, (b), (d) a magnified one. Annular regions: regions allowed at 68% C.L. by a top-pair tagged-photoproduction cross-section measurement, in photoproduction region PhP_I (7), with experimental uncertainties 12% (dark green), 15% (light green), and 18% (yellow). Light-blue area: region allowed by the measurements of the branching ratio and CP asymmetry of $B \to X_s\gamma$ decays, using the results from [11]. Darker-blue area: same as previous, but using the results from [12].

of allowed regions are identical in the neighborhood of the origin (i.e., the SM), which is consistent with the individual-coupling bounds we obtain being the same at both energies.

Also shown in the figure are the regions in the κ–$\widetilde{\kappa}$ plane allowed by the branching ratio and CP asymmetry for the process $B \to X_s\gamma$, in both the form obtained from [11], and the form from [12]. The difference in area between these two regions hardly needs to be emphasized. We remark, however, that even the smaller region resulting from [12] is not completely contained in the annular regions determined by top-pair photoproduction, which results in a significant reduction of the allowed parameter space.

5 Final remarks

In this note we summarize the results of our analysis [1] of top-pair photoproduction in semileptonic mode in pe collisions at the LHeC and FCC-he. Our main results are the limits (9) on $\widetilde{C}_{\varphi q}^{(-)33}$ (δf_V^L), and those on $\widetilde{C}_{uB\,r}^{33}$, $\widetilde{C}_{uB\,i}^{33}$ (κ, $\widetilde{\kappa}$), (11), and the two-dimensional allowed regions for κ, $\widetilde{\kappa}$ in figure 2. We also made a detailed comparison of our results to those from ATLAS and CMS from [13–15].

Based on our results, we expect the LHeC to provide limits on $\widetilde{C}_{\varphi q}^{(-)33}$ (δf_V^L) similar to those from the HL-LHC. We also expect the LHeC to obtain limits on $\widetilde{C}_{uB}^{33}$ stronger than those from the HL-LHC. These will then be the strongest until the operation of e^-e^+ colliders begins. Both sets of limits will constitute an important contribution to future global analyses. The FCC-he can yield improved sensitivity to $\widetilde{C}_{\varphi q}^{(-)33}$ and $\widetilde{C}_{uB}^{33}$, relative to that of the LHeC, from substantially larger statistics and improved systematics.

The recent strong results on limits on top electromagnetic dipole moments by the LHC collaborations [14, 15] suggest, however, that we should upgrade our analysis of top photoproduction in pe colliders by including appropriate differential cross sections. An enhanced background rejection from a more robust multivariate analysis would also help strengthen the bounds on top couplings. These extensions to our analysis

are currently in progress; we will report the results elsewhere.

1. A. Bouzas, F. Larios, "Top quark effective couplings from top-pair tagged photoproduction in pe^- collisions," Phys. Rev. D **105**, 115002 (2022), https://doi.org/10.1103/PhysRevD.105.115002 [arXiv:2111.04723 [hep-ph].
2. P. Agostini *et al.* [LHeC and FCC-he Study Group], "The Large Hadron-Electron Collider at the HL-LHC," J. Phys. G **48** (2021) 110501, https://doi.org/10.1088/1361-6471/abf3ba [arXiv:2007.14491 [hep-ex]].
3. Q. H. Cao, B. Yan, C. P. Yuan and Y. Zhang, polarization in ZZ production at hadron colliders," Phys. Rev. D **102** (2020) 055010, https://doi.org/doi:10.1103/PhysRevD.102.055010 [arXiv:2004.02031 [hep-ph]].
4. A. Kozachuk and D. Melikhov, "Constraints on the anomalous Wtb couplings from B-physics experiments," Symmetry **12** (2020) 1506, https://doi.org/doi:10.3390/sym12091506 [arXiv:2004.13127 [hep-ph]].
5. I. A. Sarmiento-Alvarado, Antonio O. Bouzas, F. Larios, "Analysis of top-quark charged-current coupling at the LHeC," J. Phys. G **42** (2015) 085001, https://doi.org/10.1088/0954-3899/42/8/085001 [arXiv:1412.6679 [hep-ph]].
6. S. Dutta, A. Goyal, M. Kumar and B. Mellado, "Measuring anomalous Wtb couplings at e^-p collider," Eur. Phys. J. C **75** (2015) 577, https://doi.org/doi:10.1140/epjc/s10052-015-3776-z [arXiv:1307.1688 [hep-ph]].
7. A. Bouzas, F. Larios, "Probing $tt\gamma$ and ttZ couplings at the LHeC," Phys. Rev. D **88** (2013) 094007, https://doi.org/10.1103/PhysRevD.88.094007 [arXiv:1308.5634 [hep-ph]].
8. A. A. Billur, M. Köksal and A. Gutiérrez-Rodríguez, "Improved sensitivity on the electromagnetic dipole moments of the top quark in $\gamma\gamma$, $\gamma\gamma^*$ and $\gamma^*\gamma^*$ collisions at the CLIC," Phys. Rev. D **96** (2017) 056007, https://doi.org/doi:10.1103/PhysRevD.96.056007 [arXiv:1702.03708 [hep-ph]].
9. M. Köksal, A. A. Billur, A. Gutiérrez-Rodríguez and M. A. Hernández-Ruíz, "Sensitivity measuring expected on the electromagnetic anomalous couplings in the $t\bar{t}\gamma$ vertex at the FCC-he," Int. J. Mod. Phys. A **35** (2020) 2050178, doi:10.1142/S0217751X2050178X [arXiv:1905.02564 [hep-ph]].
10. A. Bouzas, F. Larios, "Electromagnetic dipole moments of the top quark," Phys. Rev. D **87** (2013) 074015, https://doi.org/10.1103/PhysRevD.87.074015 [arXiv:1212.6575 [hep-ph]].
11. J. L. Hewett and T. G. Rizzo, "Using $b \to s\gamma$ to probe top quark couplings," Phys. Rev. D **49** (1994) 319, doi:10.1103/PhysRevD.49.319 [arXiv:hep-ph/9305223 [hep-ph]].
12. J. Aebischer, A. Crivellin, M. Fael and C. Greub, "Matching of gauge invariant dimension-six operators for $b \to s$ and $b \to c$ transitions," JHEP **05** (2016) 037, doi:10.1007/JHEP05(2016)037 [arXiv:1512.02830 [hep-ph]].
13. CMS collaboration, "Search for anomalous Wtb couplings and flavour-changing neutral currents in t-channel single top quark production in pp collisions at $\sqrt{s}$ = 7 and 8 TeV," JHEP **02** (2017) 028, https://doi.org/10.1007/JHEP02(2017)028.
14. CMS collaboration, "Measurement of the inclusive and differential $t\bar{t}\gamma$ cross sections in the dilepton channel and effective field theory interpretation in proton-proton collisions at $\sqrt{s} = 13$ TeV," JHEP **05** (2022) 091, https://doi.org/10.1007/JHEP05(2022)091.
15. ATLAS collaboration, "Prospects for the measurement of $t\bar{t}\gamma$ with the upgraded ATLAS detector at the High-Luminosity LHC," CERN report ATL-PHYS-PUB-2018-049, Dec. 2018.
16. B. Grzadkowski, M. Iskrzyński, M. Misiak, J. Rosiek, "Dimension-Six Terms in the Standard Model Lagrangian," JHEP **10** (2010) 085, https://doi.org/10.1007/JHEP10(2010)085 [arXiv:1008.4884 [hep-ph]].
17. C. Zhang, "Effective field theory approach to top-quark decay at next-to-leading order in QCD," Phys. Rev. D **90** (2014) 014008, https://doi.org/10.1103/PhysRevD.90.014008 [arXiv:1404.1264 [hep-ph]].
18. E. E. Jenkins, A. V. Manohar and M. Trott, "Naive Dimensional Analysis Counting of Gauge Theory Amplitudes and Anomalous Dimensions," Phys. Lett. B **726**, 697-702 (2013) https://doi.org/10.1016/j.physletb.2013.09.020 [arXiv:1309.0819 [hep-ph]].
19. J. A. Aguilar Saavedra et al., "Interpreting top-quark LHC measurements in the standard-model effective field theory," CERN report CERN-LPCC-2018-01 (2018) [arXiv:1802.07237 [hep-ph]]
20. J. Alwall, R. Frederix, S. Frixione, V. Hirschi, F. Maltoni, O. Mattelaer, H.-S. Shao, T. Stelzer, P. Torrielli, M. Zaro, "The automated computation of tree-level and next-to-leading order differential cross sections, and their matching to parton shower simulations," J. High Energy Phys. **07** (2014) 079, https://doi.org/10.1007/JHEP07(2014)079 [arXiv:1405.0301 [hep-ph]].
21. T. Sjostrand, S. Mrenna, P. Skands, "Pythia 6.4 Physics and Manual," J. High Energy Phys. **05** (2006) 26, https://doi.org/10.1088/1126-6708/2006/05/026 [arXiv:hep-ph/0603175].
22. J. de Favereau, C. Delaere, P. Demin, A. Giammanco, V. Lemaitre, A. Mertens, M. Selvaggi, "DELPHES 3: a modular framework for fast simulation of a generic collider experiment," J. High Energy Phys. **02** (2014) 057 https://doi.org/10.1007/JHEP02(2014)057 [arXiv:1307.6346 [hep-ph]].